Science of the Total Environment 907 (2024) 167818

Contents lists available at ScienceDirect

Science of the Total Environment

journal homepage: www.elsevier.com/locate/scitotenv

Development of surface observation-based two-step emissions adjustment and its application on CO, NO_x, and SO_2 emissions in China and South Korea

Eunhye Kim [a,b], Hyun Cheol Kim [c,d], Byeong-Uk Kim [e], Jung-Hun Woo [f], Yang Liu [b], Soontae Kim [a,b,*]

[a] Department of Environmental & Safety Engineering, Ajou University, Suwon 16499, South Korea
[b] Gangarosa Department of Environmental Health, Rollins School of Public Health, Emory University, Atlanta, GA 30322, USA
[c] Air Resources Laboratory, National Oceanic and Atmospheric Administration, College Park, MD 20740, USA
[d] Cooperative Institute for Satellite Earth System Studies, University of Maryland, College Park, MD 20740, USA
[e] Georgia Environmental Protection Division, Atlanta, GA 30354, USA
[f] Department of Civil and Environmental Engineering, Konkuk University, Seoul 05029, South Korea

HIGHLIGHTS

- Upwind and downwind emissions during the last 6 years were adjusted with TEA.
- The adjusted downwind emissions reflect upwind emission changes.
- NMBs of CO, NO_x, and SO_2 concentrations were improved ±114 % to ±10 %.
- Upwind CO & SO_2 emission changes decreased the downwind concentrations by 21 & 14 %.
- The emission decrease rates in both areas were 2–7 %/year during the last 3 years.

GRAPHICAL ABSTRACT

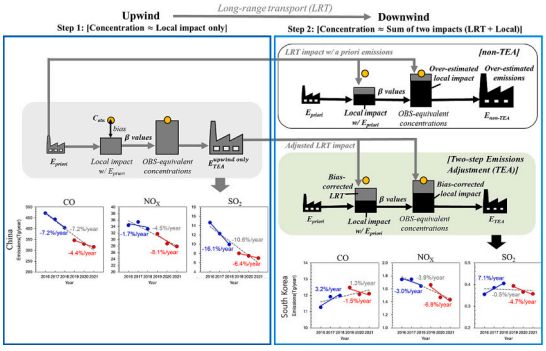

ARTICLE INFO

Editor: Pavlos Kassomenos

Keywords:
Emissions adjustment
Downwind
Long-range transport

ABSTRACT

It is challenging to estimate local emission conditions of a downwind area solely based on concentrations in the downwind area. This is because air pollutants that have a long residence time in the atmosphere can be transported over long distances and influence air quality in downwind areas. In this study, a Two-step Emissions Adjustment (TEA) approach was developed to adjust downwind emissions of target air pollutants with surface observations, considering their long-range transported emission impacts from upwind areas calculated from air quality simulations. Using the TEA approach, CO, NO_x, and SO_2 emissions were adjusted in China and South

Abbreviations: CAPSS, Clean Air Policy Support System; CMAQ, Community Multi-scale Air Quality model; CREATE, Comprehensive Regional Emissions inventory for Atmospheric Transport Experiment; EI, emissions inventory; KORUS, Korea–United States Air Quality; LRT, Long-Range Transport; MEIC, Multi-resolution Emission Inventory for China; NAIR, National Air Emission Inventory and Research Center; TEA, Two-step Emissions Adjustment; WRF, Weather Research and Forecasting model.

* Corresponding author at: Department of Environmental & Safety Engineering, Ajou University, Suwon 16499, South Korea.
E-mail address: soontaekim@ajou.ac.kr (S. Kim).

https://doi.org/10.1016/j.scitotenv.2023.167818
Received 26 July 2023; Received in revised form 22 September 2023; Accepted 11 October 2023
Available online 18 October 2023

Transported impact
Surface observations

Korea between 2016 and 2021 based on existing bottom-up emissions inventories. Simulations with the adjusted emissions showed that the 6-year average normalized mean biases of the monthly mean concentrations of CO, NO_x, and SO_2 improved to 0.3 %, −2 %, and 2 %, respectively, in China, and to 5 %, 7 %, and 4 %, respectively, in South Korea. When analyzing the emission trends, it was estimated that the annual emissions of CO, NO_x, and SO_2 in China decreased at a rate of 7.2 %, 4.5 %, and 10.6 % per year, respectively. The decrease rate of emissions for each of these pollutants was similar to that of ambient concentrations. When considering upwind emission impacts in the emissions adjustment, CO emissions increased by 1.3 %/year in South Korea, despite CO concentrations in the country decreasing during the study period. During the study period, NO_x and SO_2 emissions in South Korea decreased by 3.9 % and 0.5 %/year, respectively. Moreover, the TEA approach can account for drastic short-term emission changes (e.g., social distancing due to COVID-19). Therefore, the TEA approach can be used to adjust emissions and improve reproducibility of concentrations of air pollutants suitable for health studies for areas where upwind emission impacts are significant.

1. Introduction

The ambient concentrations of $PM_{2.5}$, SO_2, and NO_x in Northeast Asia have declined recently (Ali et al., 2023; Bae et al., 2023; Lee et al., 2022; Zhai et al., 2021). Previous studies reported that this downward trend resulted from emission reductions by strict emission control policies and social issues such as the COVID-19 pandemic (Bae et al., 2021; Hasnain et al., 2023; Yao et al., 2023; Zhang et al., 2023). These studies have reached their conclusions by examining the impact of emission changes on air pollutant concentrations indirectly by excluding non-emission impacts (e.g., meteorology). However, direct analysis of emission changes is non-trivial and challenging due to uncertainties in actual emission estimation.

Actual emissions for a specific year are often represented in a bottom-up emissions inventory (EI) that is updated regularly (e.g., yearly). However, some emission sources may be missing from EIs during the data collection process (Ou et al., 2018). For example, in Northeast Asia, CO emissions have been significantly underestimated because of missing sources (Gaubert et al., 2020; Park et al., 2021; Qu et al., 2022). In addition, inaccurate emission factors and insufficient activity data may lead to uncertainties in the emissions data (Streets et al., 2003; Zhao et al., 2011). Another limitation of bottom-up EIs is that it takes time to collect and verify emissions data, so there is a lag between the year represented by an EI and the year when the EI is published. For example, the inventory years of the latest public version of the Multi-resolution Emission Inventory for China (MEIC) and the Regional Emission Inventory in Asia version 3 (REASv3), the two most up-to-date and available EIs in Northeast Asia, are 2017 and 2015, respectively (Zheng et al., 2018; Kurokawa and Ohara, 2020). However, it is difficult to estimate emission changes with these EIs in recent years (e.g., 2020 and 2021) because of the rapid changes in Northeast Asia, including anthropogenic emission changes due to the establishment of social distancing guidelines during the COVID-19 outbreak (Uno et al., 2020; Zheng et al., 2018; Han et al., 2020; Huang et al., 2021; Itahashi et al., 2022; Kang et al., 2020). Furthermore, more intricate changes in anthropogenic emissions are projected for Northeast Asia, as the imperative for emission reductions to improve air quality and mitigate climate change is undeniable (Chishti and Patel, 2023; Li et al., 2023; Shi et al., 2023; Chishti et al., 2021). These bottom-up EIs may be suitable for modeling study on past periods, but using them to understand recent air quality is challenging.

To overcome the aforementioned limitations of bottom-up EIs, previous studies have attempted to adjust emissions with satellite observations (Bae et al., 2020b; Elguindi et al., 2020; Emmons et al., 2004; Fu et al., 2022; Gaubert et al., 2020; Salmon et al., 2018; Qu et al., 2022). However, satellite observation data are available only for daylight hours, excluding thermal radiation-based information such as fire emissions. Moreover, satellite data have their own limitations such as missing data due to clouds, in addition to limited spatiotemporal resolution (Barré et al., 2021; Zoogman et al., 2011). Due to these limitations, some studies have attempted to adjust emissions using surface observed concentrations and simulated concentrations with bottom-up EIs as an alternative (Bae et al., 2020a; Bergamaschi et al., 2000; Feng et al., 2020; Kasibhatla et al., 2002; Wang et al., 2013). However, in these studies, the emission impact from upwind areas was not accounted for when estimating local emissions based on concentrations.

In a downwind area, in addition to its own local emissions, the concentrations of air pollutants can also be affected by emissions from upwind areas depending on meteorological conditions (Itahashi et al., 2022; Kim et al., 2021a; Uno et al., 2020). The concentrations of air pollutants with a short residence time, such as NO_x, are mainly affected by local emissions, while those with a long residence time, such as CO, stay in the atmosphere for several months and can be transported long distances. Therefore, uncertainty in upwind emissions should be considered prior to adjusting emissions in a downwind area. Similarly, when long-term emission trends in a downwind area are estimated, those for upwind areas should be considered. Inverse modeling may be used to solve this problem by adjusting emissions to improve model performance in simulating concentrations of both the upwind and downwind areas simultaneously (Lee et al., 2011; Yumimoto et al., 2014). However, the calculation process is complicated, and various emission adjustment factors that do not match reality may be included (Brioude et al., 2011; Mendoza-Dominguez and Russell, 2000).

In this study, the Two-step Emissions Adjustment (TEA) approach was developed and applied. TEA is an emission adjustment method that could update emissions in downwind as well as upwind areas. Using the TEA approach, the long-term trends of emissions in China and South Korea, designated as upwind and downwind areas respectively, were analyzed for 2016–2021 including the COVID-19 outbreak period. In addition, the emissions adjusted from two different EIs with the TEA approach were compared to demonstrate that the proposed approach can estimate a posteriori (or adjusted) emissions to simulate air pollutant concentrations comparable to the observations.

This novel approach enables us to estimate emissions in downwind areas by considering the long-range transport (LRT) of air pollutants. The ability to adjust emissions for air pollutants with long residence times distinguishes it from previous research. The TEA approach is an effective method that allows for the rapid estimation of realistic emissions using surface observations which will be helpful for policymakers when developing regional and local air pollution control plans. Since air pollutant concentrations simulated with adjusted emissions are much more consistent with the observations, the TEA-based modeling results will be useful for health studies, as reported by Ma et al. (2016).

2. Methodology

The source-receptor relationships between target air pollutants and concentrations of those air pollutants in an area were established with photochemical air quality model simulations and surface observations in upwind and downwind areas. In this study, China and South Korea were chosen as the target areas for emission adjustments based on the TEA method. Air pollutant concentrations in China have significantly decreased recently due to the implementation of strict emission control policies and the impact of social distancing in response to COVID-19

(Kim et al., 2021a, b; Uno et al., 2020; Zhang et al., 2023). In addition, China's emissions of air pollutants are anticipated to continue to decrease, supported by greenhouse gas emission reductions (Chishti and Patel, 2023; Li et al., 2023). These changes in China's emissions have also had an impact on the air pollutant concentrations in neighboring areas, including South Korea (Bae et al., 2021; Uno et al., 2020). Therefore, it was determined that the application of TEA would be suitable for emission adjustments in both China and South Korea. Geographically, China and South Korea are in the westerly zone. The Yellow Sea, where there are few anthropogenic emission sources, is located between the two countries. The target pollutants selected in this study are CO, NO_2, and SO_2. The TEA approach in which upwind emissions are adjusted prior to adjusting downwind emissions is introduced in Section 2.1. For the emissions adjustment, an air quality simulation was conducted based on existing EIs for the upwind and downwind areas first (Sections 2.2–2.3). Then, emissions were adjusted using the surface observations (Section 2.4). Last, the validity of the TEA approach was assessed by comparing adjusted emissions based on two different unadjusted EIs (Section 2.5). Further details are explained in each section.

2.1. Two-step emissions adjustment (TEA) approach

The TEA approach adjusts emissions in both upwind and downwind areas by considering the LRT of air pollutants. Fig. 1 shows how the TEA approach is different from the non-TEA adjustment method that adjusts downwind emissions without taking the impact of LRT into account. Over- and under-estimation of downwind emissions in a non-TEA method is plausible due to uncertainties in transported impacts from upwind areas. Biases in modeled concentrations in a downwind area can be reduced by adjusting the local emissions. However, when upwind emissions are updated — thus changing the impact to the downwind area — downwind emissions should be recalculated.

The TEA approach updates the influence of LRT on simulated downwind concentrations prior to the adjustment of downwind emissions. First, the emissions of China (the upwind area in this study) were adjusted using surface observations (Section 2.4). Then, the emissions of the target pollutants in South Korea (i.e., the downwind area) were adjusted by utilizing the same methodology as the upwind area. In doing so, the adjusted upwind impact can be included when adjusting downwind emissions.

This approach is similar to previous studies (Bae et al., 2020b; Elguindi et al., 2020; Gaubert et al., 2020; Qu et al., 2022; Xing et al., 2022) in such a way that bottom-up emissions were constrained in observations. However, a major difference in the TEA approach when compared to previous approaches is that upwind emission impacts (i.e., LRT) were considered in downwind areas when adjusting emissions from the downwind area. Another major difference is that previous studies mostly relied on satellite data, which are limited to daytime information when developing top-down emissions. In contrast, this study utilized long-term hourly resolved surface CO, NO_x, and SO_2 observational data, covering not only daytime but also nighttime periods.

The TEA approach is useful for adjusting emissions but still has limitations on adjustments in upwind areas, especially boundary areas of the outer domain as the concentrations over grid cells can be influenced by regional background conditions which are not adjustable in this approach. In addition, the adjusted emissions can be influenced by uncertainties in the input data such as meteorology and emissions, and the chemical transport model itself. Considering uncertainties inherent in the emissions adjustment method, the long-term trend of emissions was highlighted in the downwind area rather than attempting to quantify the emission rates. Based on this approach, changes in the long-term CO, NO_x, and SO_2 emissions in the upwind and downwind areas were estimated from 2016 to 2021. The study period was divided into two shorter periods: the pre-COVID-19 period (P1: 2016–2018) and the post-COVID-19 period (P2: 2019–2021). In addition, the impact of emission changes in the upwind area on air quality in the downwind area was evaluated (i.e., air quality improvements in South Korea owing to China's emission reduction). The detailed configuration of the scenario used in this study is presented in Table S1.

2.2. Emissions inventories

The Korea–United States Air Quality (KORUS) v5 from Konkuk University (Woo et al., 2020) and Clean Air Policy Support System (CAPSS) 2017 from the National Air Emission Inventory and Research Center (NAIR) were used as the EIs for the a priori emissions for China

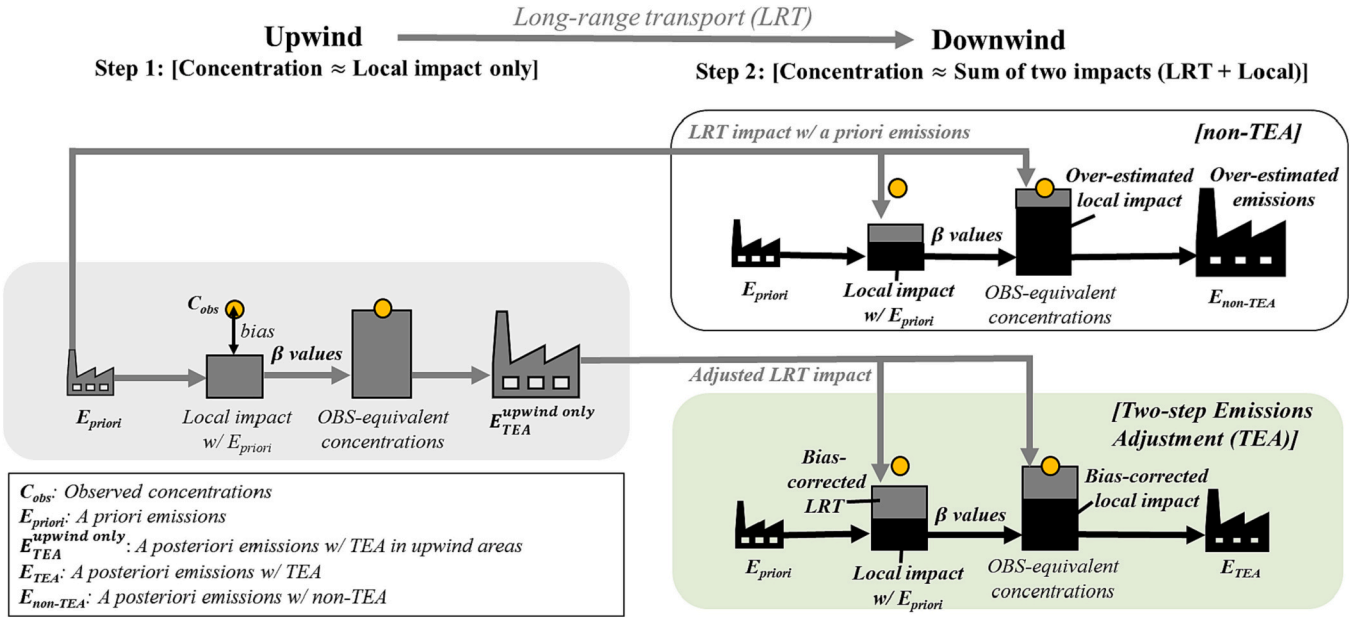

Fig. 1. Illustrative comparison of Two-step Emissions Adjustment (TEA) and non-TEA approaches. It was assumed that the bias of the simulated concentration was caused by the uncertainty of the a priori (i.e., unadjusted) emissions (E_{priori}). Based on this assumption, the a posteriori (i.e., adjusted) emissions ($E_{posteriori}$) were estimated to accurately simulate the observed concentrations. The β values that represent the emission-concentration conversion rate are explained in Section 2.4.

and South Korea, respectively. Chinese emissions of CO, SO_x, and NO_x were 168.7 Tg/year, 29.9 Tg/year, and 21.2 Tg/year, respectively, as reported in the Comprehensive Regional Emissions inventory for Atmospheric Transport Experiment (CREATE) 2015. At the same time, KORUS v5 reported that Chinese emissions of CO, SO_x, and NO_x were 141.9 Tg/year, 13.3 Tg/year, and 22.5 Tg/year, respectively, in 2016. Meanwhile, MEIC 2017, the most up-to-date EI of China, reported that Chinese emissions of CO, SO_x, and NO_x were 136.2 Tg/year, 10.5 Tg/year, and 22.0 Tg/year, respectively, in 2017 (Zheng et al., 2018). CREATE 2015 was also used for cross-validation of the TEA approach in Section 3.5.

In CAPSS 2017, the emissions of CO, SO_x, and NO_x of South Korea were 0.8 Tg/year, 0.3 Tg/year, and 1.2 Tg/year, respectively (Choi et al., 2021). In South Korea, the three main sources of CO emissions include road, non-road mobile, and biomass burning, accounting for 78 % of the total emissions. The main sources of SO_x emissions are energy production, industrial processes, and manufacturing, accounting for 81 % of the total emissions. NO_x emissions mainly originate from road and non-road mobile sources, manufacturing, and energy production, accounting for 86 % of the total emissions. The emission densities (in tons per year per km^2) of CO, NO_x, and SO_2 in China are 1.8, 0.2, and 0.5 times those in South Korea, respectively.

2.3. Air quality simulation

Meteorological input data for the air quality simulation were prepared in two steps. First, the Weather Research and Forecasting model (WRF; Skamarock et al., 2008) v3.9.1 was run with initial and boundary conditions from the Final Analysis data (FNL) provided by the National Center for Environmental Prediction (NCEP). Second, because the Community Multi-scale Air Quality model (CMAQ) v5.3.1 was used as the chemical transport model, the WRF outputs were converted into CMAQ-ready meteorological input files using Meteorology-Chemistry Interface Processor (MCIP) v4.3. Hourly weather simulation results were verified by comparing them with observed data from 82 observation stations of the Meteorological Assimilation and Data Ingest System (MADIS) in China and South Korea. The EIs were processed using the Sparse Matrix Operator Kernel Emission model (SMOKE; Benjey et al., 2001) v3.1. Biogenic emissions were calculated using the Model of Emissions of Gases and Aerosols from Nature (MEGAN; Guenther et al., 2006) based on vegetation data. The results of the hemispherical model of CMAQ v5.3 beta2, provided by the United States Environmental Protection Agency (U.S. EPA, 2020), were used as boundary conditions.

Concentrations of air pollutants during the study period were simulated with CMAQ using the prepared meteorological dataset and unadjusted emissions. The detailed WRF and CMAQ configurations used in this study are presented in Table 1. As for the simulation areas (see Fig. 2), Northeast Asia, including China and South Korea, is included in Domain 1 while South Korea (the downwind area) is focused on Domain 2. Boundary conditions for Domain 2 were extracted from the simulated results of concentrations for Domain 1. Modeling results for Domains 1 and 2 were used to adjust the emissions in the upwind and downwind areas, respectively.

Table 1
Model configurations and input data for air quality simulations.

	Options	Module
WRF v3.9.1 (Meteorology)	Microphysics	WSM6 (Hong and Lim, 2006)
	Longwave & shortwave radiation	RRTMG (Iacono et al., 2008)
	PBL scheme	YSU (Hong and Lim, 2006)
CMAQ v5.3.1 (Chemistry)	Chemical mechanism	SAPRC07 (Hutzell et al., 2012)
	Chemical solver	EBI (Hertel et al., 1993)
	Aerosol module	AERO6 (Simon and Bhave, 2012)

For emissions adjustment and verification of simulated air quality concentrations, hourly observations from the China National Environmental Monitoring Center (CNEMC), South Korean Air Monitoring Station (AMS), and AirKorea (https://www.airkorea.or.kr) were used. Fig. 2 shows the locations of observation sites in this study. During 2016, the total number of monitoring stations available for China and South Korea was 1332 and 311, respectively.

2.4. Emissions adjustment with surface observations

In this study, it was assumed that the bias of the simulated concentration was attributed to the uncertainty in the a priori emissions (E_{priori}). An emissions inventory selected can be the a priori emissions in this study. Under this assumption, the a posteriori emissions ($E_{posteriori}$) were estimated by adjusting E_{priori} with emission-concentration conversion rates (β) to accurately simulate the observed concentrations (C_{obs}). In previous studies, the β value of a target area of certain pollutants was assumed to be 1, and the ratios of observed and simulated concentrations (C_{priori}) were applied directly to the a priori emissions (Bae et al., 2020a; Kim et al., 2021b). As the concentration over a downwind area is affected not only by its own emissions but also by emissions from surrounding areas, β values may vary by period, area, the residence time of a pollutant, and background concentrations. Lamsal et al. (2011) attempted to estimate more realistic β values by calculating the emission-concentration sensitivity with 15 % perturbed emissions in the target area. Meanwhile, Kim et al. (2021b) calculated the β values for each specific region and time.

This study adopted the approach described by Kim et al. (2021b) to calculate β values by each area and month. To calculate the local sensitivity of air pollutant concentrations to the emissions changes, perturbed emissions (E_{sens}) were set by multiplying the a priori emissions of CO, NO_x, and SO_2 with the corresponding constant values of 1.5, 1.3, and 0.7. These constants were calculated by averaging the ratios of observed concentrations to simulated concentrations with the unadjusted emissions over time. Then, the a posteriori emissions were calculated as a sum of the a priori emissions and the ratio of the difference between the observed concentration and the simulated concentration with E_{priori}, ($C_{obs} - C_{priori}$), and the β value (Eqs. (1) and (2)).

$$\beta_{s,t} = \left(C_{sens} - C_{priori}\right)_{s,t} \Big/ \left(E_{sens} - E_{priori}\right)_{s,t} \quad (1)$$

$$E_{posteriori} = E_{priori} + \left[\left(C_{obs} - C_{priori}\right)_{s,t}\right] \Big/ \beta_{s,t} \quad (2)$$

where

$\beta_{s,t}$: Emission-concentration conversion rate at an area s over a time period t

C_{sens}: Simulated concentration of the air pollutant using E_{sens}

C_{priori}: Simulated concentration of the air pollutant using E_{priori}

E_{sens}: Perturbed emissions of the air pollutant to estimate emission-concentration sensitivity

E_{priori}: A priori emissions of the target air pollutant from an area s

$E_{posteriori}$: A posteriori emissions of a target air pollutant from an area s

C_{obs}: Observed concentration of the air pollutant

Subsequently, the monthly β values were calculated to estimate monthly emission variations in 309 prefectures and 17 provinces for China and South Korea, respectively. The size of each prefecture in China and province in South Korea ranges from 1000 to 27,000 km^2 and from 500 to 19,000 km^2, respectively. It should be noted that air quality monitoring stations are distributed unevenly so that one modeling grid cell may have multiple stations while some modeling grid cells may not have any stations. Therefore, comparisons between observed and simulated concentrations at each monitor location can cause many-to-one or one-to-many matching, potentially leading to uncertainties in model-observation comparisons depending on the number of monitors in each modeling grid cell. To reduce this type of uncertainty, this study

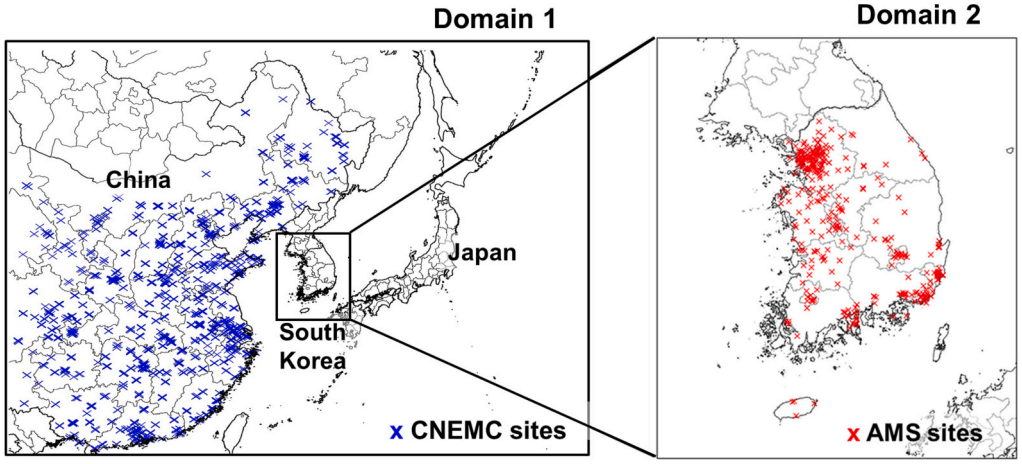

Fig. 2. Domains for air quality simulation and location of observation sites in China (left) and South Korea (right), as of 2016.

adopted the approach used in Bae et al. (2020a) where the β values were calculated first by averaging observed data from observational stations in one grid and then averaging the observed and simulated concentrations for each prefecture or province. If there are no observation sites in a province, a monthly β value of 1 was assumed for that province. Generally, observation sites are located in highly polluted areas, so it is believed that the observed data in each province can accurately represent the concentration levels of that province.

2.5. Validation of the emissions adjustment

To show the effectiveness of the emissions adjustment approach proposed in this study, two validation steps were taken. First, in addition to KORUS v5 (E_{priori}), another EI, CREATE 2015 (E^*_{priori}), was adjusted with the TEA approach for China to examine how the emission constraint with the surface observations can generally be applied with different EIs. Secondly, emissions adjusted with the TEA and non-TEA approaches were compared for the downwind area. The correlation of adjusted emissions between E_{TEA} and E^*_{TEA}, which represent TEA-based adjusted emissions for E_{priori} and E^*_{priori}, in South Korea was compared to the correlation of adjusted emissions between $E_{non-TEA}$ and $E^*_{non-TEA}$, which represent non-TEA-based adjusted emissions for E_{priori} and E^*_{priori}, respectively.

3. Results and discussion

3.1. Model performance evaluation of meteorological factors

The meteorological model performance was evaluated with observational data from China and South Korea (Fig. S1). During the study period, the average 2-m air temperatures in China and South Korea were around 15.0 °C. Simulated 2-m temperatures showed biases around −1.3 °C. The Index of Agreement (IOA) and the Pearson correlation coefficient (R) for the monthly average 2-m air temperatures were 0.99 and 1.0, respectively. The average value of observed 10-m wind speeds was 2.9 m/s during the study period. Simulated 10-m wind speeds showed biases around 0.3 m/s. The IOA and R values for the monthly average 10-m wind speeds were 0.6 and 0.7, respectively.

3.2. Concentration changes after emission adjustments

To validate the resultant emissions estimated with the TEA approach, simulated concentrations with and without the emission adjustment were compared with the observations. The C_{priori} of NO_2 and SO_2 for 2021 showed overestimation in China with normalized mean biases (NMBs) of 5.4 % and 193.3 % for NO_2 and SO_2, respectively. The C_{priori} of NO_2 and SO_2 for 2021 in South Korea were similar to the C_{obs}. The resulting NMBs for NO_2 and SO_2 were −0.8 % and −0.1 %, respectively. On the other hand, the NMB of the C_{priori} for CO in 2021 was negative at −37.3 % and −67.5 % in China and South Korea, respectively. This is consistent with other studies, that is, CO emissions in Northeast Asia are significantly underestimated in the bottom-up EIs (Park et al., 2021; Qu et al., 2022; Tang et al., 2019).

In China, during 2016–2021, the average NMBs of the C_{priori} were −46 % and −7 % for CO and NO_2, respectively, while the average NMB for SO_2 was 114 %. After the emissions adjustment, the NMBs for CO, NO_2, SO_2 were improved to 0.3 %, −2 %, and 2 %, respectively. The R values were also improved after the emission adjustment from 0.70 to 0.99 for CO, from 0.77 to 0.97 for NO_2, and from 0.52 to 1.00 for SO_2.

In South Korea, the model performance was improved after the emissions adjustment. For CO, the period average NMBs were −70 % without the adjustment (C_{priori}), and 5 % after the emission adjustment (C_{TEA}). For NO_2, the period average NMBs were −12 % without adjustment and 7 % after the second adjustment (i.e., upwind and downwind emission adjustment as shown in Fig. 1). When only the upwind emissions were adjusted, the period average NMBs for CO and NO_2 concentrations ($C^{upwind\ only}_{TEA}$) in the downwind area became −57 % and −11 %, respectively. It was noted that the model performance statistics for the NO_2 simulations with and without the upwind emission adjustment were similar in South Korea. This may be due to the short residence time of NO_2 that prevents it from traveling long distances from upwind to downwind areas (Lange et al., 2022; Beirle et al., 2011). For SO_2, the period average NMB was −19 % in C_{priori}, and 4 % after the emissions adjustment while the NMB increased to 23 % when the upwind emissions were only adjusted. The recent significant decrease in SO_2 emissions in the upwind area intensified the underestimation of SO_2 concentrations ($C^{upwind\ only}_{TEA}$) in South Korea as shown in Fig. 3. However, the annual NMB of SO_2 decreased after the downwind emissions were adjusted in the second step (C_{TEA} in South Korea in Fig. 3). These results demonstrate the effectiveness of the TEA approach for adjusting emissions of downwind areas to improve model performance.

The simulated concentrations with a posteriori emissions were compared to the observed concentrations in Fig. 4. After the emissions adjustment, the simulated monthly average concentrations of CO, NO_2, and SO_2 in China in 2021 decreased by 33 %, 23 %, and 60 %, respectively, compared to those in 2016 ($C^{upwind\ only}_{TEA}$ in Fig. 4). This is similar to the rates of reductions in the observed concentrations, 34 %, 20 %, and 59 % for CO, NO_2, and SO_2, respectively, indicating that the upwind a posteriori emissions (E_{TEA}) appropriately reflected the changes in emissions in China. In particular, the steep decrease in NO_2

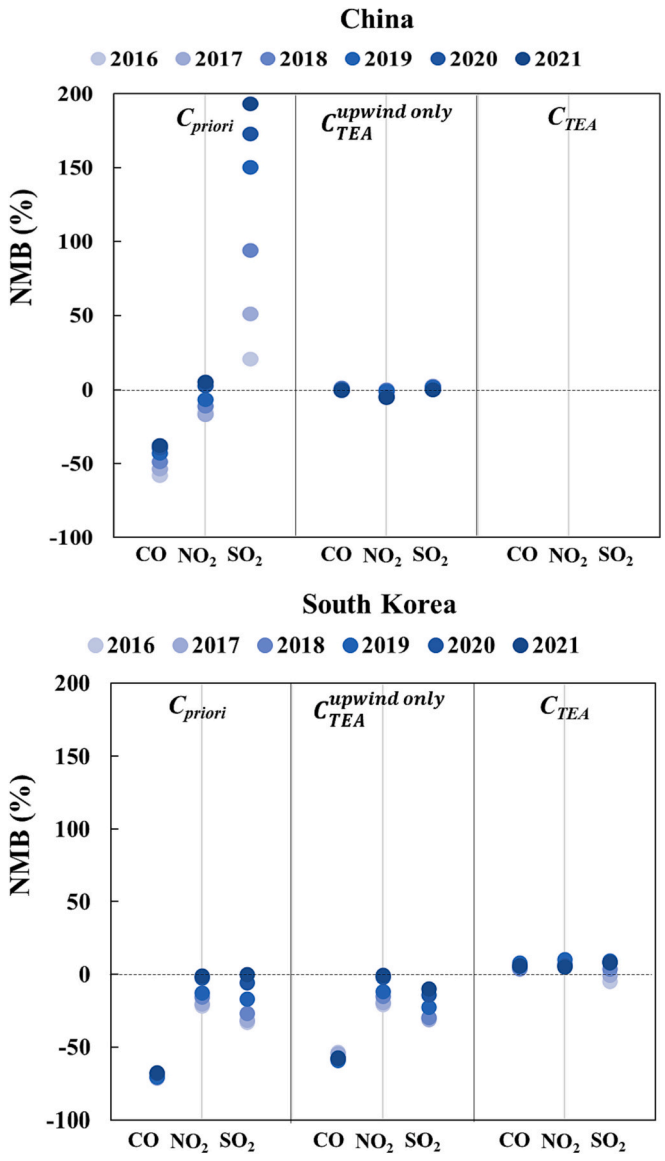

Fig. 3. The Normalized Mean Biases (NMB) of simulated concentrations for the selected air pollutants of CO, NO_2, and SO_2 in China (top) and South Korea (bottom) for each year of the study period (2016–2021). Each column shows NMB of (1) C_{priori}; concentrations with a priori emissions (left), (2) $C_{TEA}^{upwind\ only}$; concentrations with adjusted upwind emissions as the first step in the TEA approach (middle), and (3) C_{TEA}; concentrations with the final adjusted emissions in the TEA approach (right). C_{TEA} is only available for South Korea because South Korea was designated as the downwind area.

concentration during the COVID-19 lockdown in China in January 2020 was well-reproduced, similar to the findings of Kim et al. (2021b).

For C_{priori}, the changes in concentration reflect only the changes in meteorological conditions as the same emissions were used regardless of the simulation year. The average annual C_{priori} of CO, NO_2, and SO_2 in China in 2021 decreased by about 1 % compared to those in 2016 as a result of changes in meteorological conditions (red line in Fig. 4). Thus, it can be said that the recent decrease in the observed concentrations of air pollutants in China is mainly due to changes in emissions rather than in meteorology during the study period. Several studies have also reported that Chinese emissions have decreased significantly in recent years (Bae et al., 2021; Zhai et al., 2019).

In South Korea, C_TEA, with the adjusted emissions from both the upwind and downwind areas, is best at reproducing the changing trend in observed concentrations. The observed concentration of CO decreased by 12 % in 2021 compared to that in 2016, whereas the simulated CO concentration decreased by 20 % with $C_{TEA}^{upwind\ only}$ and 10 % with C_{TEA}. This means that changes in CO emissions in the upwind area reduced the concentrations by 21 % ($= C_{TEA}^{upwind\ only} - C_{priori}$) in South Korea while the local emissions in the downwind area increased the concentration by 10 % ($= C_{TEA} - C_{TEA}^{upwind\ only}$) for the period. The simulated NO_2 concentration also decreased by 2 % with $C_{TEA}^{upwind\ only}$ and 23 % with C_{TEA} in 2021 compared to 2016, showing that the C_{TEA} better reflect the change rate (−22 %) in the observed concentration. This is because NO_2 has a short residence time in the air as described above. It seems that the reduction rate of the NO_2 concentration with C_{TEA} was mostly due to changes in emissions in South Korea. The observed concentration of SO_2 decreased by 36 % in 2021 compared to that in 2016, while the simulated concentration decreased by 18 % with $C_{TEA}^{upwind\ only}$ in South Korea. It implies that changes in SO_2 emissions in the upwind area reduced the concentrations by 14 % ($C_{TEA}^{upwind\ only} - C_{priori}$) in the downwind area. The C_{TEA} decreased by 26 % showing a lower change rate than the observed concentration change rate. It seems that the SO_2 concentration with C_{TEA} was underestimated in 2016 and overestimated in 2021 (Figs. 3 and 4), resulting in a decrease in the change rate compared to the actual change in emission.

The results in Figs. 3 and 4 indicated that in both China and South Korea, the simulated concentrations with a posteriori emissions better reproduced the observed concentrations and their trends of changes than those with a priori emissions. This confirmed the effectiveness of the proposed emissions adjustment approach. In addition, although not included as target pollutants in this study, it is possible to improve the estimation of downwind emissions of EC, a major component of $PM_{2.5}$ in Northeast Asia, through the TEA approach. This is especially relevant considering the potential for LRT.

3.3. Validation of the TEA approach

The TEA approach was validated by comparing the a posteriori emissions for the two different EIs, E_{priori} and E^*_{priori}. Before adjustment, the CO, NO_x, and SO_2 emissions from E^*_{priori} (CREATE 2015) were relatively higher than those of the E_{priori} (KORUS v5) by 17 %, 11 %, and 93 %, respectively, in the upwind area (Fig. S2). After adjustment, the differences between E_{TEA}, which represents the adjusted emissions for E_{priori}, and E^*_{TEA}, which represents the adjusted emissions for E^*_{priori}, were as minor as within ±10 % for all pollutants (CO = 10 %, NO_x = 6 %, and SO_2 = 8 %) in the upwind area. The correlation coefficients (R) between the adjusted monthly emissions were also improved, with values of 0.96 (CO), 0.98 (NO_x), and 1.00 (SO_2), compared to the R-values before the adjustments (CO = 0.86, NO_x = 0.83, and SO_2 = 0.92). In addition, the simulated concentrations of all pollutants with the adjusted emissions (C_{TEA} and C^*_{TEA}) showed better agreement with the observed concentrations compared to those with a priori emissions as shown in Fig. S3. Thus, this convergence confirmed that the emission adjustment with the surface observations applied in this study can successfully constrain emissions to simulate air pollutant concentrations well-matched with the observations for different EIs as the a priori emissions.

In South Korea (i.e., the downwind area), the convergence of the adjusted emissions based on the TEA approach was compared to that of the emissions based on the non-TEA approach. The relative differences between the $E_{non-TEA}$ and $E^*_{non-TEA}$ were 2 %, 1 %, and 33 % for CO, NO_X, and SO_2, respectively (Fig. S4). On the other hand, the relative differences between the E_{TEA} and E^*_{TEA} were 4 %, 0 %, and 6 % for CO, NO_X, and SO_2, respectively. In addition, the correlation coefficient of SO_2 emissions between E_{TEA} and E^*_{TEA} (0.90) was higher than that between $E_{non-TEA}$ and $E^*_{non-TEA}$ (0.84). It is presumed that a relatively small difference in CO emissions in the a priori emissions and a short residence time of NO_2 in the atmosphere make insignificant differences in the a

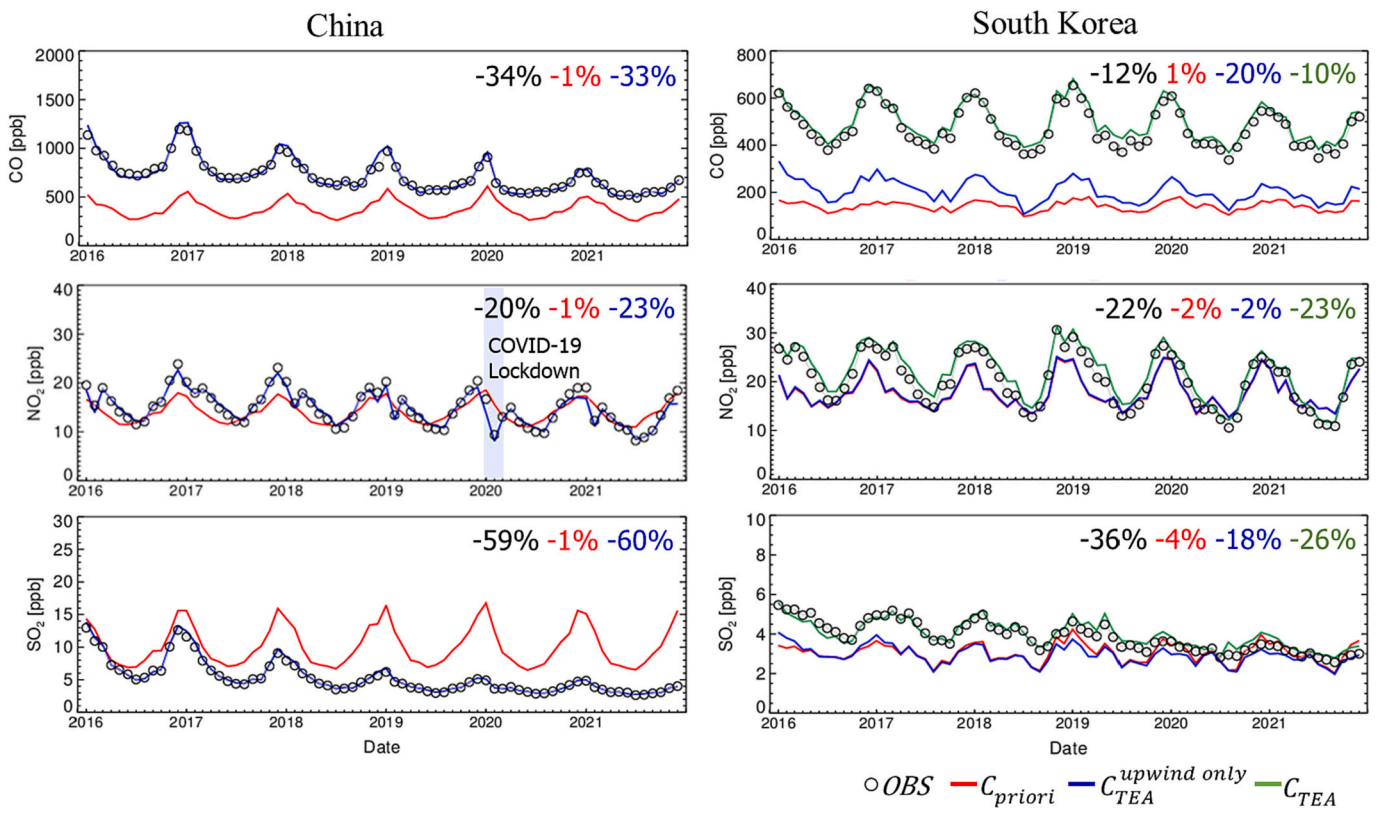

Fig. 4. Comparison of trends in concentrations of CO (top), NO_2 (middle), and SO_2 (bottom) in China (left) and South Korea (right) according to the emission adjustment: circles indicate observations, red lines denote simulations with a priori emissions (C_{priori}), blue lines denote simulations with adjusted Chinese emissions ($C_{TEA}^{upwind\ only}$), and the green lines denote simulations with adjusted emissions from both China and South Korea (C_{TEA}). Each number represents the annual percentage change in 2021 compared to 2016.

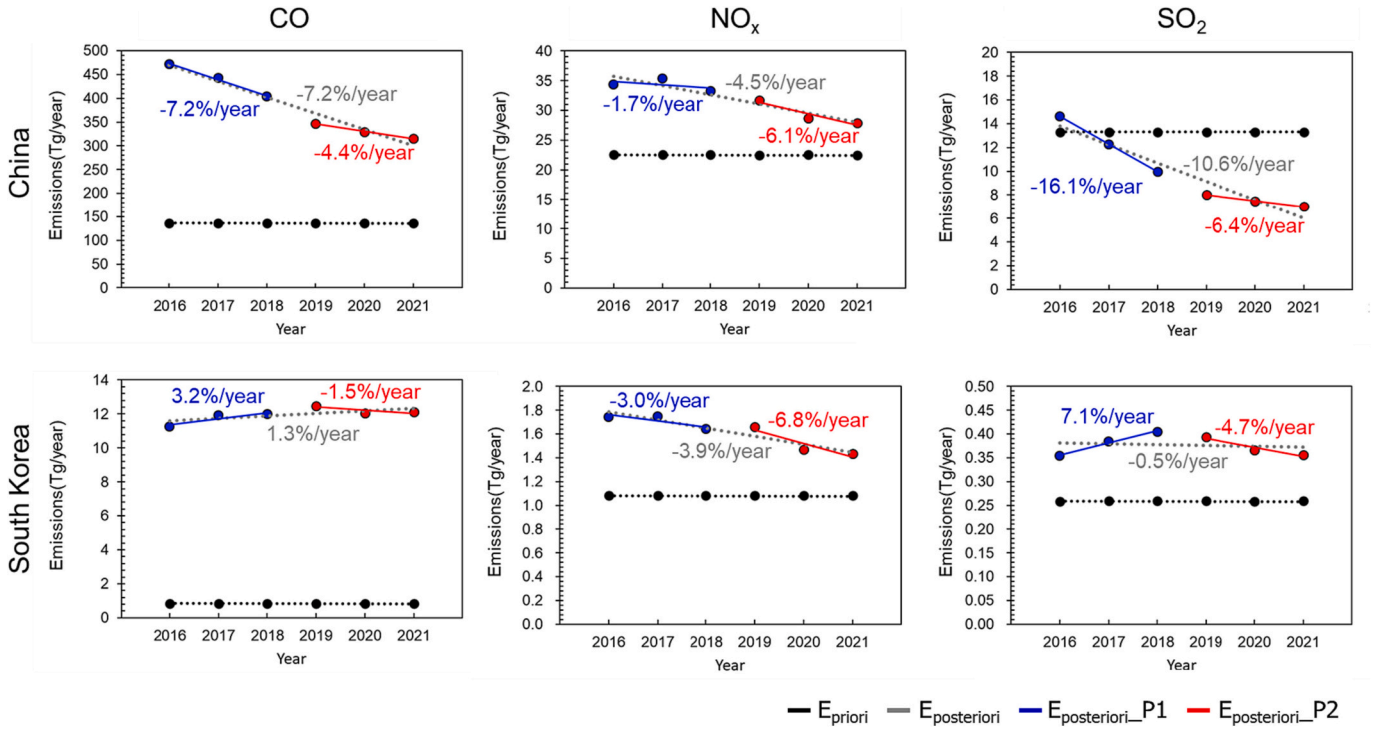

Fig. 5. Comparison of emissions of CO (left), NO_x (middle), and SO_2 (right) and their trends in China (top) and South Korea (bottom): Black circles represent a priori emissions, red and blue circles represent a posteriori emissions for the first half (P1) and the second half (P2) of the study period, respectively. The slope of each trend line indicates the annual emission change trend. The dotted line is the trend line for the entire period. The number (%/year) is the annual average rate of change in emissions, calculated based on each trend line.

posteriori emissions.

The simulated concentrations with the adjusted emissions using the TEA approach (C_{TEA}) showed higher agreement with the observed concentrations compared to the simulated concentrations with the adjusted emissions using the non-TEA approach ($C_{non-TEA}$) (Fig. S5). For SO_2, the NMBs were −33 % and −3 % for $C_{non-TEA}$ and C_{TEA}, respectively. The correlation coefficients with the observations were −0.32 and 0.94 for $C_{non-TEA}$ and C_{TEA}, respectively. Therefore, the TEA approach is advantageous in adjusting emissions in a downwind area when long-range transport of air pollutants from upwind areas plays a significant role in determining air quality over a downwind area.

3.4. Annual emissions and trends after the application of TEA

The a posteriori emissions (i.e., E_{TEA}) and their trends over time were analyzed in China and South Korea. As shown in Fig. 5, China's a posteriori CO emissions in 2016 were 471.9 Tg/year, 3.5 times higher than the a priori emissions (136.5 Tg/year). In the same year, South Korea's a posteriori CO emissions were 11.3 Tg/year which is 14 times higher than the a priori emissions (0.8 Tg/year). This means that a priori CO emissions in China and South Korea were underestimated, which was also reported by previous studies (Park et al., 2021; Qu et al., 2022). However, it should be noted that this study did not adjust emissions from North Korea. If emissions from North Korea were adjusted, the underestimation of emissions in China and South Korea would have been alleviated because recent studies (i.e., Chong et al., 2023; Jung et al., 2022) showed that CO and NO_x emissions from North Korea were underestimated.

In China, the annual average a posteriori CO emissions decreased at a rate of 7.2 %/year from 2016 to 2021, resulting in a 33 % reduction in 2021 compared to 2016. When dividing the study period into two parts (i.e., the pre-COVID-19 period (P1: 2016–2018) and the post-COVID-19 period (P2: 2019–2021)), Chinese a posteriori CO emissions decreased more rapidly during P1 (−7.2 %/year) than P2 (−4.4 %/year). The annual average a posteriori CO emissions of South Korea increased slightly at a rate of 1.3 %/year over the entire period, resulting in a 7 % increase in CO emissions in 2021 compared to 2016. Meanwhile, CO emissions increased during P1 (3.2 %/year) but decreased during P2 (−1.5 %/year). The trend of changes in observed CO concentrations in the upwind and downwind areas may appear similar since CO is a pollutant that travels over long distances. However, the trend of CO emission change in China (the upwind area) appeared to be the opposite of that in South Korea (the downwind area) during P1 in this study. This implies that estimating emission changes in the downwind area solely based on observations is difficult unless the impacts of upwind emissions in the downwind area are considered.

In 2016, China's a posteriori NO_x emissions were 34.4 Tg/year, 1.5 times the a priori emissions (22.5 Tg/year). In South Korea, it was estimated to be 1.7 Tg/year which is 1.5 times the a priori emissions (1.1 Tg/year). This means that a priori NO_x emissions might be underestimated, which was also suggested by Goldberg et al. (2019). The annual trends of a posteriori emissions showed that Chinese NO_x emissions decreased by 4.5 %/year on average over the period, which is 19 % lower in 2021 compared to 2016. This emission reduction occurred more sharply during P2 (−6.1 %/year) than P1 (−1.7 %/year). Xu et al. (2023) and Zheng et al. (2018) have reported a downward trend of NO_x emissions in China. South Korea's a posteriori NO_x emissions decreased by an average of 3.9 %/year over the study period, which is 18 % lower in 2021 compared to 2016. The emission reduction occurred more rapidly during P2 (−6.8 %/year) than during P1 (−3 %/year), like in China. During P2, the reduction rates of NO_x emissions in South Korea were following the same trend as China, possibly due to the impact of social distancing during the COVID-19 outbreak and strong emission regulations to improve air quality (Kang et al., 2020; Lv et al., 2023).

Chinese a posteriori SO_2 emissions were 14.6 Tg/year in 2016, showing little difference from the a priori emissions (13.3 Tg/year) compared to other pollutants. However, the emissions decreased by −10.6 %/year on average over the period, resulting in a 52 % reduction in 2021 compared to 2016. This significant reduction in emissions appears to be the result of the implementation of SO_2-focused reduction policies such as those in the 13th Five-Year Plan in China (Jiao et al., 2017). Zheng et al. (2018) reported a 59 % decrease in SO_2 emissions in China in 2017 compared to 2013. In this study, the rate of decrease was slower during P2 (−6.4 %/year) when compared to P1 (−16.1 %/year). Meanwhile, South Korea's a posteriori SO_2 emissions were estimated to be 0.35 Tg/year that is higher than a priori emissions (0.26 Tg/year). The a posteriori SO_2 emissions increased during P1 (7.1 %/year) but decreased again during P2 (−4.7 %/year), resulting in a similar level of SO_2 emissions in 2016 and 2021 in South Korea. Considering the results shown in the previous section where the SO_2 concentrations in South Korea in 2021 were overestimated by approximately 8.6 % with a posteriori emissions, it is possible that the SO_2 emissions were overestimated as well.

In 2016, the a posteriori emission densities of CO, NO_x, and SO_2 in China were 49.2 Tg/million km^2, 3.6 Tg/million km^2, and 1.5 Tg/million km^2, respectively, whereas in South Korea the emission densities of CO, NO_x, and SO_2 were 112.6 Tg/million km^2, 17.5 Tg/million km^2, and 3.5 Tg/million km^2, respectively. Thus, the emission densities in South Korea are 2.3 times (CO), 4.9 times (NO_x), and 2.3 times (SO_2) higher than those in China. In 2021, the a posteriori emission densities of CO, NO_x, and SO_2 in China were 32.9 Tg/million km^2, 2.9 Tg/million km^2, and 0.7 Tg/million km^2, respectively, whereas in South Korea they were 121.0 Tg/million km^2, 14.3 Tg/million km^2, and 3.6 Tg/million km^2 for CO, NO_x, and SO_2, respectively. As a result, the emission densities of these pollutants in South Korea were 3.7 times (CO), 4.9 times (NO_x), and 4.9 times (SO_2) higher than those in China in 2021. This implies that recent changes in emissions in China and South Korea have increased the relative importance of domestic emissions control in South Korea, especially considering the higher population density that exposes more people to air pollutants.

In terms of the spatial distribution of emissions (Fig. 6), the a posteriori emissions of CO, NO_x, and SO_2 were all reduced in 2021 compared to 2016 in China. Meanwhile, those in South Korea showed different trends depending on the pollutants: CO emissions increased in most provinces, but NO_x emissions decreased overall. Additionally, SO_2 emissions showed increases and decreases in different provinces while the overall emission trend in South Korea showed little change.

3.5. Monthly variations after the application of TEA

Fig. 7 shows that, in 2016, a posteriori CO emissions during winter in China were higher than in other seasons, similar to EI. However, in 2021, the emissions in summer were higher than those in other seasons. This is possibly due to Chinese emission control policies for the wintertime residential heating to reduce $PM_{2.5}$ concentrations (Wang et al., 2019; Zheng et al., 2018). Meanwhile, the a posteriori CO emissions in South Korea in summer have slightly increased in recent years.

The a posteriori NO_x emissions are lower than the a priori emissions in summer compared to spring and winter in both China and South Korea. Such seasonal variability of NO_x emissions has also been reported in precedent studies (Mijling et al., 2013). Low NO_x emissions during February in China seem to be due to factory closures and reduced vehicle operation during the Lunar New Year (Tan et al., 2009). In China, there was a significant decrease in NO_x emissions from January to March 2020 when compared with those for the same period of previous years. In particular, the a posteriori NOx emissions in February 2020 were 1.4 Tg/month, 30 % lower than those of the same period in the previous year (2.0 Tg/month) (Fig. 7). This is due to the lockdown during the COVID-19 outbreak (Bauwens et al., 2020; Chu et al., 2021; Kim et al., 2021b). In February 2021, the NO_x emissions returned to pre-COVID-19 levels, 1.8 Tg/month, as reported in previous studies (Itahashi et al., 2022; Kim et al., 2021b; Zhang et al., 2020). In South Korea, a notable decrease in

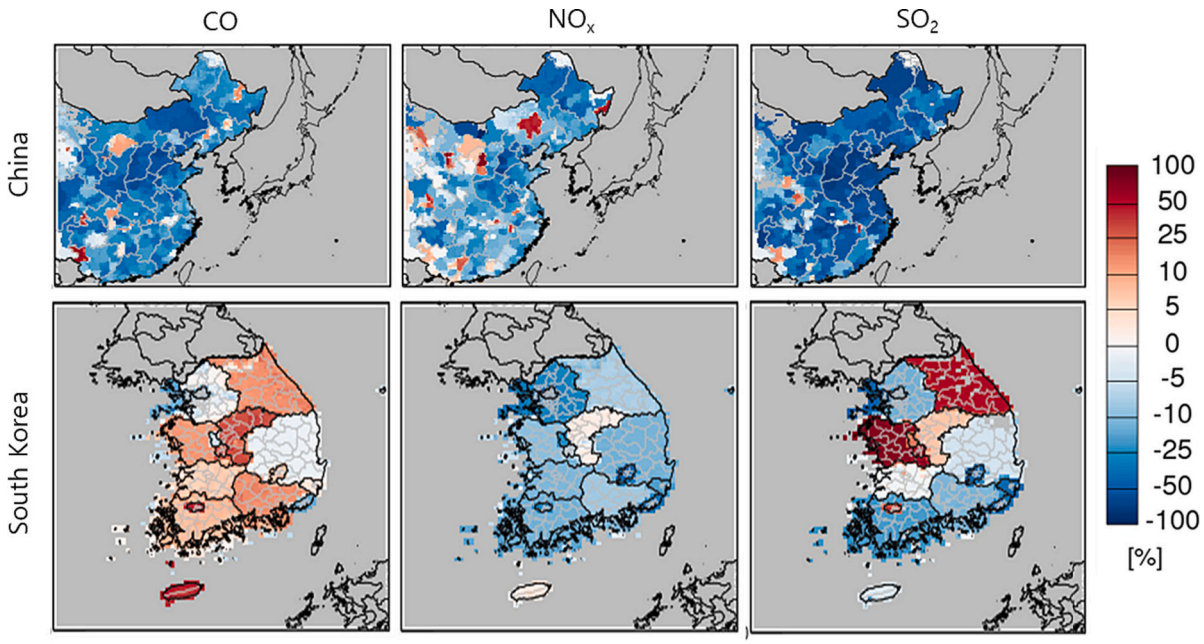

Fig. 6. Relative rates of change in a posteriori emissions in 2021 compared to 2016 in China (top) and South Korea (bottom): CO (left), NO_x (middle), and SO_2 (right).

NO_x emissions compared with the same period of the previous year occurred in March 2020 and 2021. This is presumed to be attributed to the impact of implementing emission reduction policies, such as the Seasonal Management of $PM_{2.5}$ during the spring and winter seasons, along with the enforcement of social distancing during the COVID-19 pandemic (Kang et al., 2020; Lee et al., 2020; Son et al., 2020).

Chinese a posteriori SO_2 emissions have steadily decreased since 2016. Moreover, the decrease in emissions is larger in the spring and winter seasons than in the summer season. From 2019 (i.e., P2), SO_2 emissions are high in summer and low in spring and winter, which contrasts with the seasonal variability of emissions in 2016. On the other hand, in South Korea, a posteriori SO_2 emissions in summer have recently increased. As shown previously, CO emissions also increased in summer, which may be due to the increased activities of emission sources that emit both CO and SO_2 such as coal-fired power plants.

4. Conclusion

In this study, a Two-step Emissions Adjustment (TEA) approach that adjusts upwind emissions prior to adjusting downwind emissions to account for the effects of LRT on air pollutants was developed. As for validation of the TEA approach, it was demonstrated that air quality simulation results with the adjusted emissions matched well with short-term (i.e., COVID-19) and long-term variations of CO, SO_2, and NO_x in China and South Korea during the period of 2016–2021.

The emission reduction rates in the upwind area (i.e., China) were similar to those in ambient concentrations of air pollutants since self-contributions to the ambient concentrations are predominant in the upwind area. On the other hand, the TEA approach revealed that changes in CO and SO_2 emissions in the upwind area reduced the concentrations in South Korea, the downwind area, by 21 % and 14 %, respectively, in 2021 compared to those of 2016 while the observed CO and SO_2 concentrations in the downwind area decreased by 12 % and 36 %, respectively, during the period. It implies that the impacts of upwind emissions should be considered for the air pollutants of which atmospheric residence time is long enough for regional transport when emission conditions in a downwind area are estimated. In the case of NO_x, the upwind emission impact was insignificant in the downwind area due to its relatively short residence time in the atmosphere. The emission reductions were more pronounced in the spring and winter seasons than in the summer season for both China and South Korea. This may result from policy implementations to manage the high $PM_{2.5}$ concentrations that frequently occur during the cold seasons.

The TEA approach that was introduced made it possible to estimate changes in emissions quickly and accurately not only for downwind areas but also upwind areas. This methodology can also be applied in regions beyond Northeast Asia, especially where regional transport of air pollutants is significant to determine local air quality. In addition, the simulated concentrations based on adjusted emissions demonstrated greater reproducibility with the observed concentrations than those based on unadjusted emissions. This is because the TEA approach follows a top-down approach that estimates emissions inversely from observations. In this study, the average NMBs of simulated CO, SO_2, and NO_2 concentrations with the adjusted emissions showed significant improvement as follows: −46 % → 0.3 %, 114 % → 2 %, and −7 % → -2 %, respectively, in China, and −70 % → 5 %, −19 % → 4 %, and −12 % → 7 %, respectively, in South Korea. As the simulated concentrations based on the adjusted emissions closely matched the observed concentrations, it can be expected that the adjusted emissions from the TEA approach can also be utilized to simulate concentrations of air pollutants for health risk assessments related to air pollution exposure.

In this study, emissions were adjusted to better replicate observed concentrations rather than estimate actual emissions. It should be noted that adjusted emissions are subject to change depending on the air quality modeling system adopted. Therefore, instead of focusing on the magnitude of emissions estimated in this study, long-term trends of CO, NO_x, and SO_2 emissions were highlighted. Additionally, uncertainties may arise when applying this approach in boundary areas where no observations are available beyond the location. Discrepancies between observed and modeled concentrations, including boundary condition-induced biases, are often attributed to uncertainties in local emissions over the areas. In areas where obtaining ground observations is challenging, exploring alternative data sources such as satellite observations can be beneficial.

CRediT authorship contribution statement

Eunhye Kim: Conceptualization, Investigation, Visualization,

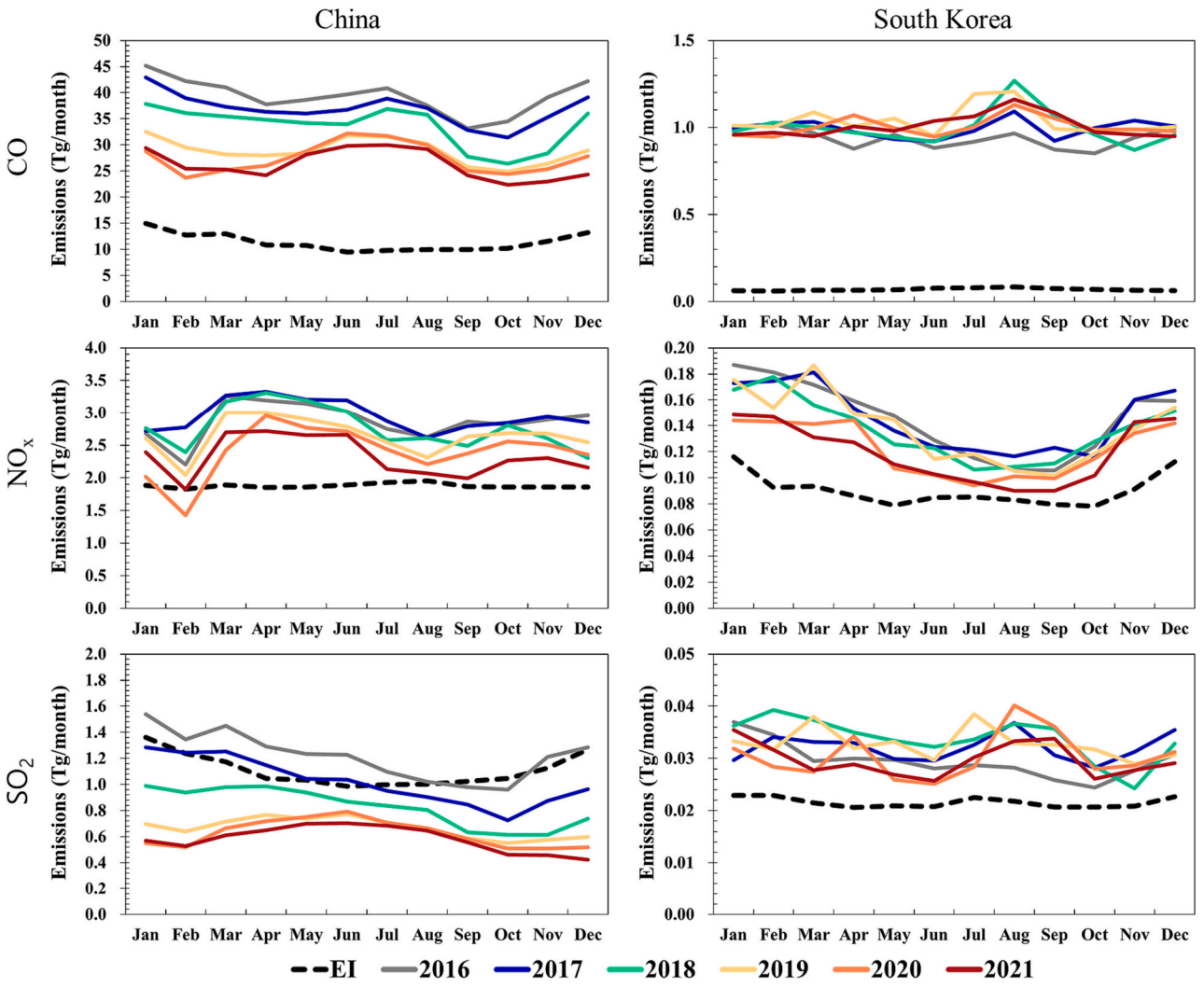

Fig. 7. Changes in monthly emissions of CO (top), NO_x (middle), and SO_2 (bottom) in China (left) and South Korea (right): Dotted line represents the a priori emissions and each solid line represents the a posteriori emissions in 2016 (gray), 2017 (blue), 2018 (green), 2019 (yellow), 2020 (orange), and 2021 (red).

Writing- Original draft

Hyun Cheol Kim: Conceptualization, Software

Byeong-Uk Kim: Writing- Reviewing & Editing

Jung-Hun Woo: Data curation

Yang Liu: Writing- Reviewing & Editing

Soontae Kim: Writing- Original draft, Supervision

Declaration of generative AI and AI-assisted technologies in the writing process

During the preparation of this work, the author(s) utilized ChatGPT to enhance their English writing. Following the use of this tool/service, the author(s) reviewed and edited the content as necessary and take full responsibility for the publication's content.

Declaration of competing interest

The authors declare that they have no known competing financial interests or personal relationships that could have appeared to influence the work reported in this paper.

Data availability

Data will be made available on request.

Acknowledgments

This work was supported by the National Air Emission Inventory and Research Center (NAIR) in South Korea and the Samsung Advanced Institute of Technology. HCK was partially supported by NOAA grant NA19NES4320002. The scientific results and conclusions, as well as any views or opinions expressed herein, are those of the author(s) and do not necessarily reflect the views of NOAA or the Department of Commerce. The authors thank the National Institute of Environmental Research (NIER), South Korea, for providing surface air quality observation data. The authors also thank Dr. Barron Henderson from US EPA for providing HCMAQ-based boundary conditions.

Appendix A. Supplementary data

Supplementary data to this article can be found online at https://doi.org/10.1016/j.scitotenv.2023.167818.

References

Ali, M.A., Huang, Z., Bilal, M., Assiri, M.E., Mhawish, A., Nichol, J.E., de Leeuw, G., Almazroui, M., Wang, Y., Alsubhi, Y., 2023. Long-term $PM_{2.5}$ pollution over China: identification of $PM_{2.5}$ pollution hotspots and source contributions. Sci. Total Environ. 893 (164871).

Bae, C., Kim, H.C., Kim, B., Kim, Y., 2020a. Updating Chinese SO_2 emissions with surface observations for regional air-quality modeling over East Asia. Atmos. Environ. 228, 117416.
Bae, C., Kim, H.C., Kim, B.-U., Kim, S., 2020b. Surface ozone response to satellite-constrained NO_x emission adjustments and its implications. Environ. Pollut. 258, 113469.
Bae, M., Kim, B.-U., Kim, H.C., Kim, J., Kim, S., 2021. Role of emissions and meteorology in the recent $PM_{2.5}$ changes in China and South Korea from 2015 to 2018. Environ. Pollut. 270, 116233.
Bae, M., Kang, Y.-H., Kim, E., Kim, S., Kim, S., 2023. A multifaceted approach to explain short-and long-term $PM_{2.5}$ concentration changes in Northeast Asia in the month of January during 2016–2021. Sci. Total Environ. 880, 163309.
Barré, J., Petetin, H., Colette, A., Guevara, M., Peuch, V.-H., Rouil, L., Engelen, R., Inness, A., Flemming, J., García-Pando, C.P., Bowdalo, D., Meleux, F., Geels, C., Christensen, J.H., Gauss, M., Benedictow, A., Tsyro, S., Friese, E., Struzewska, J., Kaminski, J.W., Douros, J., Timmermans, R., Robertson, L., Adani, M., Jorba, O., Joly, M., Kouznetsov, R., 2021. Estimating lockdown-induced European NO_2 changes using satellite and surface observations and air quality models. Atmos. Chem. Phys. 21 (9), 7373–7394.
Bauwens, M., Compernolle, S., Stavrakou, T., Müller, J.-F., van Gent, J., Eskes, H., Levelt, P.F., van der, A.R., Veefkind, J.P., Vlietinck, J., Yu, H., Zehner, C., 2020. Impact of coronavirus outbreak on NO_2 pollution assessed using TROPOMI and OMI observations. Geophys. Res. Lett. 47 e2020GL087978, e2020.
Beirle, S., Boersma, K.F., Platt, U., Lawrence, M.G., Wagner, T., 2011. Megacity emissions and lifetimes of nitrogen oxides probed from space. Science 333 (6050), 1737–1739.
Benjey, W., Houyoux, M.R., Susick, J.W., 2001. Implementation of the SMOKE emission data processor and SMOKE tool input data processor in models-3. In: Presented at the Emission Inventory Conference, Denver, CO, US EPA.
Bergamaschi, P., Hein, R., Heimann, M., Crutzen, P.J., 2000. Inverse modeling of the global CO cycle: 1. Inversion of CO mixing ratios. J. Geophys. Res. 105, 1909–1927.
Brioude, J., Kim, S.-W., Angevine, W.M., Frost, G.J., Lee, S.-H., McKeen, S.A., Trainer, M., Fehsenfeld, F.C., Holloway, J.S., Ryerson, T.B., Williams, E.J., Petron, G., Fast, J.D., 2011. Top-down estimate of anthropogenic emission inventories and their interannual variability in Houston using a mesoscale inverse modeling technique. J. Geophys. Res. 116, D20305.
Chishti, M.Z., Patel, R., 2023. Breaking the climate deadlock: leveraging the effects of natural resources on climate technologies to achieve COP26 targets. Res. Policy 82, 103576.
Chishti, M.Z., Ahmad, M., Rehman, A., Khan, M.K., 2021. Mitigations pathways towards sustainable development: assessing the influence of fiscal and monetary policies on carbon emissions in BRICS economies. J. Clean. Prod. 292, 126035.
Choi, S.W., Bae, C.H., Kim, H.C., Kim, T., Lee, H.K., Song, S.J., Jang, J.P., Lee, K.B., Choi, S.A., Lee, H.J., Park, Y., Park, S.Y., Kim, Y.M., Yoo, C., 2021. Analysis of the National Air Pollutant Emissions Inventory (CAPSS 2017) Data and Assessment of Emissions based on Air Quality Modeling in the Republic of Korea. Asian J. Atmos. Environ. 15 (4), 114–141.
Chong, H., Lee, S., Cho, Y., Kim, J., Koo, J.-H., Kim, Y.P., Kim, Y., Woo, J.-H., Ahn, D.H., 2023. Assessment of air quality in North Korea from satellite observations. Environ. Int. 171, 107708.
Chu, B., Zhang, S., Liu, J., Ma, Q., He, H., 2021. Significant concurrent decrease in $PM_{2.5}$ and NO_2 concentrations in China during COVID-19 epidemic. Environ. Sci. (China) 99, 346–353.
Elguindi, N., Granier, C., Stavrakou, T., Darras, S., Bauwens, M., Cao, H., Chen, C., Denier van der Gon, H.A.C., Dubovik, O., Fu, T.M., Henze, D.K., Jiang, Z., Keita, S., Kuenen, J.J.P., Kurokawa, J., Liousse, C., Miyazaki, K., Müller, J.-F., Qu, Z., Solmon, F., Zheng, B., 2020. Intercomparison of magnitudes and trends in anthropogenic surface emissions from bottom-up inventories, top-down estimates, and emission scenarios. Earth's Future 8 (8), e2020EF001520.
Emmons, L.K., Deeter, M.N., Gille, J.C., Edwards, D.P., Attié, J.-L., Warner, J., Ziskin, D., Francis, G., Khattatov, B., Yudin, V., Lamarque, J.-F., Ho, S.-P., Mao, D., Chen, J.S., Drummond, J., Novelli, P., Sachse, G., Coffey, M.T., Hannigan, J.W., Gerbig, C., Kawakami, S., Kondo, Y., Takegawa, N., Schlager, H., Baehr, J., Ziereis, H., 2004. Validation of measurements of pollution in the troposphere (MOPITT) CO retrievals with aircraft in situ profiles. J. Geophys. Res. 109, D03309.
Feng, S., Jiang, F., Wu, Z., Wang, H., Ju, W., Wang, H., 2020. CO emissions inferred from surface CO observations over China in December 2013 and 2017. J. Geophys. Res. 125 (7), e2019JD031808.
Fu, Y., Sun, W., Fan, D., Zhang, Z., Hao, Y., 2022. An assessment of China's industrial emission characteristics using satellite observations of XCO_2, SO_2, and NO_2. Atmos. Pollut. Res. 13 (8), 101486.
Gaubert, B., Emmons, L.K., Raeder, K., Tilmes, S., Miyazaki, K., Arellano Jr., A.F., Elguindi, N., Granier, C., Tang, W., Barré, J., Worden, H.M., Buchholz, R.R., Edwards, D.P., Franke, P., Anderson, J.L., Saunois, M., Schroeder, J., Woo, J.-H., Simpson, I.J., Blake, D.R., Meinardi, S., Wennberg, P.O., Crounse, J., Teng, A., Kim, M., Dickerson, R.R., He, H., Ren, X., Pusede, S.E., Diskin, G.S., 2020. Correcting model biases of CO in East Asia: impact on oxidant distributions during KORUS-AQ. Atmos. Chem. Phys. 20, 14617–14647.
Goldberg, D.L., Saide, P.E., Lamsal, L.N., de Foy, B., Lu, Z., Woo, J.-H., Kim, Y., Kim, J., Gao, M., Carmichael, G., Streets, D.G., 2019. A top-down assessment using OMI NO_2 suggests an underestimate in the NO_x emissions inventory in Seoul, South Korea, during KORUS-AQ. Atmos. Chem. Phys. 19, 1801–1818.
Guenther, A., Karl, T., Harley, P., Wiedinmyer, C., Palmer, P.I., Geron, C., 2006. Estimates of global terrestrial isoprene emissions using MEGAN (Model of Emissions of Gases and Aerosols from Nature). Atmos. Chem. Phys. 6 (11), 3181–3210.
Han, B.S., Park, K., Kwak, K.-H., Park, S.-B., Jin, H.-G., Moon, S., Kim, J.-W., Baik, J.-J., 2020. Air quality change in Seoul, South Korea under COVID-19 social distancing: focusing on $PM_{2.5}$. Int. J. Environ. Res. Public Health 17, 6208.
Hasnain, A., Sheng, Y., Hashmi, M.Z., Bhatti, U.A., Ahmed, Z., Zha, Y., 2023. Assessing the ambient air quality patterns associated to the COVID-19 outbreak in the Yangtze River Delta: a random forest approach. Chemosphere 314, 137638.
Hertel, O., Berkowicz, R., Christensen, J., Hov, Ø., 1993. Test of two numerical schemes for use in atmospheric transport-chemistry models. Atmos. Environ. 27 (16), 2591–2611.
Hong, S.Y., Lim, J.O.J., 2006. The WRF single-moment 6-class microphysics scheme (WSM6). Asia-Pac. J. Atmos. Sci. 42 (2), 129–151.
Huang, X., Ding, A., Gao, J., Zheng, B., Zhou, D., Qi, X., Tang, R., Wang, J., Ren, C., Nie, W., Chi, X., Xu, Z., Chen, L., Li, Y., Che, F., Pang, N., Wang, H., Tong, D., Qin, W., Cheng, W., Liu, W., Fu, Q., Liu, B., Chai, F., Davis, S.J., Zhang, Q., He, K., 2021. Enhanced secondary pollution offset reduction of primary emissions during COVID-19 lockdown in China. Natl. Sci. Rev. 18, nwaa137.
Hutzell, W.T., Luecken, D.J., Appel, W., Carter, W., 2012. Interpreting predictions from the SAPRC07 mechanism based on regional and continental simulations. Atmos. Environ. 46, 417–429.
Iacono, M.J., Delamere, J.S., Mlawer, E.J., Shephard, M.W., Clough, S.A., Collins, W.D., 2008. Radiative forcing by long-lived greenhouse gases: calculations with the AER radiative transfer models. J. Geophys. Res. 113 (D13).
Itahashi, S., Yamamura, Y., Wang, Z., Uno, I., 2022. Returning long-range $PM_{2.5}$ transport into the leeward of East Asia in 2021 after Chinese economic recovery from the COVID-19 pandemic. Sci. Rep. 12, 5539.
Jiao, J., Han, X., Li, F., Bai, Y., Yu, Y., 2017. Contribution of demand shifts to industrial SO2 emissions in a transition economy: Evidence from China. J. Clean. Prod. 164, 1455–1466.
Jung, J., et al., 2022. The impact of springtime-transported air pollutants on local air quality with satellite-constrained NO_x emission adjustments over East Asia. J. Geophys. Res. 127 (5), e2021JD035251.
Kang, Y.H., Kang, Y.-H., You, S., Bae, M., Kim, E., Son, K., Bae, C., Kim, Y., Kim, B.-U., Kim, H.C., Kim, S., 2020. The impacts of COVID-19, meteorology, and emission control policies on $PM_{2.5}$ drops in Northeast Asia. Sci. Rep. 10, 22112.
Kasibhatla, P., Arellano, A., Logan, J.A., Palmer, P.I., Novelli, P., 2002. Top-down estimate of a large source of atmospheric carbon monoxide associated with fuel combustion in Asia. Geophys. Res. Lett. 29, 6–1.
Kim, E., Kim, B.-U., Kim, H.C., Kim, S., 2021a. Direct and cross impacts of upwind emission control on downwind PM2.5 under various NH3 conditions in Northeast Asia. Environ. Pollut. 268, 115794.
Kim, H.C., Kim, S., Cohen, M., Bae, C., Lee, D., Saylor, R., Bae, M., Kim, E., Kim, B.-U., Yoon, J.-H., Stein, A., 2021b. Quantitative assessment of changes in surface particulate matter concentrations and precursor emissions over China during the COVID-19 pandemic and their implications for Chinese economic activity. Atmos. Chem. Phys. 21, 10065–10080.
Kurokawa, J., Ohara, T., 2020. Long-term historical trends in air pollutant emissions in Asia: regional emission inventory in ASia (REAS) version 3. Atmos. Chem. Phys. (20), 12761–12793 version 3.
Lamsal, L.N., et al., 2011. Application of satellite observations for timely updates to global anthropogenic NO_x emission inventories. Geophys. Res. Lett. 38.
Lange, K., Martin, R.V., Padmanabhan, A., van Donkelaar, A., Zhang, Q., Sioris, C.E., Chance, K., Kurosu, T.P., Newchurch, M.J., 2022. Variability of nitrogen oxide emission fluxes and lifetimes estimated from Sentinel-5P TROPOMI observations. Atmos. Chem. Phys. 22 (4), 2745–2767.
Lee, C., Martin, R.V., van Donkelaar, A., Lee, H., Dickerson, R.R., Hains, J.C., Krotkov, N., Richter, A., Vinnikov, K., Schwab, J.J., 2011. SO_2 emissions and lifetimes: estimates from inverse modeling using in situ and global, space-based (SCIAMACHY and OMI) observations. J. Geophys. Res. 116, D6304.
Lee, H., Park, S.J., Lee, G.R., Kim, J.E., Lee, J.H., Jung, Y., Nam, E.W., 2020. The relationship between trends in COVID-19 prevalence and traffic levels in South Korea. Int. J. Infect. Dis. 96, 399–407.
Lee, T., Go, S., Lee, Y.G., Park, S.S., Park, J., Koo, J.-H., 2022. Temporal variability of surface air pollutants in megacities of South Korea. Front. Environ. Sci. 10, 915531.
Li, S., Wang, S., Wu, Q., Zhang, Y., Ouyang, D., Zheng, H., Han, L., Qiu, X., Wen, Y., Liu, M., Jiang, Y., Yin, D., Liu, K., Zhao, B., Zhang, S., Wu, Y., Hao, J., 2023. Emission trends of air pollutants and CO_2 in China from 2005 to 2021. Earth Syst. Sci. Data 15 (6), 2279–2294.
Lv, Y., Tian, H., Luo, L., Liu, S., Bai, X., Zhao, H., Zhang, K., Lin, S., Zhao, S., Guo, Z., Xiao, Y., Yanga, J., 2023. Understanding and revealing the intrinsic impacts of the COVID-19 lockdown on air quality and public health in North China using machine learning. Sci. Total Environ. 857, 159339.
Ma, Z., Hu, X., Sayer, A.M., Levy, R., Zhang, Q., Xue, Y., Tong, S., Bi, J., Huang, L., Liu, Y., 2016. Satellite-based spatiotemporal trends in $PM_{2.5}$ concentrations: China, 2004–2013. Environ. Health Perspect. 124 (2), 184–192.
Mendoza-Dominguez, A., Russell, A.G., 2000. Iterative inverse modeling and direct sensitivity analysis of a photochemical air quality model. Environ. Sci. Technol. 34 (23), 4974–4981.
Mijling, B., van der, A.R.J., Zhang, Q., 2013. Regional nitrogen oxides emission trends in East Asia observed from space. Atmos. Chem. Phys. 13 (23), 12003–12012.
Ou, J., Zheng, J., Yuan, Z., Guan, D., Huang, Z., Yu, F., Shao, M., Louie, P.K.K., 2018. Reconciling discrepancies in the source characterization of VOCs between emission inventories and receptor modeling. Sci. Total Environ. 628, 697–706.
Park, R.J., Oak, Y.J., Emmons, L.K., Kim, C.-H., Pfister, G.G., Carmichael, G.R., Saide, P. E., Cho, S.-Y., Kim, S., Woo, J.-H., Crawford, J.H., Gaubert, B., Lee, H.-J., Park, S.-Y., Jo, Y.-J., Gao, M., Tang, B., Stanier, C.O., Shin, S.S., Park, H.Y., Bae, C., Kim, E.,

2021. Multi-model intercomparisons of air quality simulations for the KORUS-AQ campaign. Elem. Sci. Anth. 9, 00139.
Qu, Z., Henze, D.K., Worden, H.M., Jiang, Z., Gaubert, B., Theys, N., Wang, W., 2022. Sector-based top-down estimates of NO_x, SO_2, and CO emissions in East Asia. Geophys. Res. Lett. 49 (2), e2021GL096009.
Salmon, O.E., Shepson, P.B., Ren, X., He, H., Hall, D.L., Dickerson, R.R., Stirm, B.H., Brown, S.S., Fibiger, D.L., McDuffie, E.E., Campos, T.L., Gurney, K.R., Thornton, J. A., 2018. Top-down estimates of NO_x and CO emissions from Washington, D.C.-Baltimore during the WINTER campaign. J. Geophys. Res. 123 (14), 7705–7724.
Shi, X., Lei, Y., Xue, W., Liu, X., Li, S., Xu, Y., Lv, C., Wang, S., Wang, J., Yan, G., 2023. Drivers in carbon dioxide, air pollutants emissions and health benefits of China's clean vehicle fleet 2019–2035. J. Clean. Prod. 391, 136167.
Simon, H., Bhave, P.V., 2012. Simulating the degree of oxidation in atmospheric organic particles. Environ. Sci. Technol. 46 (1), 331–339.
Skamarock, W.C., Klemp, J.B., Dudhia, J., Gill, D.O., Barker, D., Duda, M.G., Huang, X.-Y., Wang, W., Powers, J.G., 2008. A Description of the Advanced Research WRF Version 3 (No. NCAR/TN-475+STR). University Corporation for Atmospheric Research. https://doi.org/10.5065/D68S4MVH.
Son, K., Son, K., Bae, M., You, S., Kim, E., Kang, Y.H., Bae, C., Kim, Y., Kim, H.C., Kim, B., Kim, S.T., 2020. Meteorological and emission influences on $PM_{2.5}$ concentration in South Korea during the seasonal management: a case of December 2019 to March 2020. J. Korean Soc. Atmos. Environ. 442–463.
Streets, D.G., Bond, T.C., Carmichael, G.R., Fernandes, S.D., Fu, Q., He, D., Klimont, Z., Nelson, S.M., Tsai, N.Y., Wang, M.Q., Woo, J.-H.-. Yarber, K.F., 2003. An inventory of gaseous and primary aerosol emissions in Asian in the year 2000. J. Geophys. Res. 108 (D21), 8809.
Tan, P.-H., Chou, C., Liang, J.-Y., Chou, C.C.-K., Shiu, C.-J., 2009. Air pollution "holiday effect" resulting from the Chinese New Year. Atmos. Environ. 43, 2114–2124.
Tang, W., Emmons, L.K., Arellano Jr., A.F., Gaubert, B., Knote, C., Tilmes, S., Buchholz, R.R., Pfister, G.G., Diskin, G.S., Blake, D.R., Blake, N.J., Meinardi, S., DiGangi, J.P., Choi, Y., Woo, J.-H., He, C., Schroeder, J.R., Suh, I., Lee, H.-J., Jo, H.-Y., Kanaya, Y., Jung, J., Lee, Y., Kim, D., 2019. Source contributions to carbon monoxide concentrations during KORUS-AQ based on CAM-chem model applications. J. Geophys. Res. 124, 2796–2822.
U.S. EPA, 2020. Policy Assessment for the Review of the Ozone National Ambient Air Quality Standards (EPA-452/R-20-001). United States Environmental Protection Agency. https://www.epa.gov/sites/production/files/2020-05/documents/o3-final_pa-05-29-20compressed.pdf.
Uno, I., Wang, Z., Itahashi, S., Yumimoto, K., Yamamura, Y., Yoshino, A., Takami, A., Hayasaki, M., Kim, B.-G., 2020. Paradigm shift in aerosol chemical composition over regions downwind of China. Sci. Rep. 10, 6450.
Wang, X., Wang, Y., Hao, J., Kondo, Y., Irwin, M., Munger, J.W., Zhao, Y., 2013. Top-down estimate of China's black carbon emissions using surface observations: sensitivity to observation representativeness and transport model error. J. Geophys. Res. 118 (11), 5781–5795.
Wang, S., Li, Y., Haque, M., 2019. Evidence on the impact of winter heating policy on air pollution and its dynamic changes in North China. Sustainability 11, 2728.
Woo, J.H., Kim, Y., Kim, H.-K., Choi, K.-C., Eum, J.-H., Lee, J.-B., Lim, J.-H., Kim, J., Seong, M., 2020. Development of the CREATE inventory in support of integrated climate and air quality modeling for Asia. Sustainability 12.
Xing, J., Li, S., Zheng, S., Liu, C., Wang, X., Huang, L., Song, G., He, Y., Wang, S., Sahu, S. K., Zhang, J., Bian, J., Zhu, Y., Liu, T.-Y., Hao, J., 2022. Rapid inference of nitrogen oxide emissions based on a top-down method with a physically informed variational autoencoder. Environ. Sci. Technol. 56 (14), 9903–9914.
Xu, J., Zhang, Z., Zhao, X., Cheng, S., 2023. Downward trend of NO_2 in the urban areas of Beijing-Tianjin-Hebei region from 2014 to 2020: comparison of satellite retrievals, ground observations, and emission inventories. Atmos. Environ. 295, 119531.
Yao, Z., Wang, Y., Qiu, X., Song, F., 2023. Impact of anthropogenic emission reduction during COVID-19 on air quality in Nanjing, China. Atmosphere 14 (4), 630.
Yumimoto, K., Uno, I., Itahashi, S., 2014. Long-term inverse modeling of Chinese CO emission from satellite observations. Environ. Pollut. 195, 308–318.
Zhai, S., Jacob, D.J., Wang, X., Shen, L., Li, K., Zhang, Y., Gui, K., Zhao, T., Liao, H., 2019. Fine particulate matter ($PM_{2.5}$) trends in China, 2013–2018: separating contributions from anthropogenic emissions and meteorology. Atmos. Chem. Phys. 19 (16), 11031–11041.
Zhai, S., Zhai, S., Jacob, D.J., Wang, X., Liu, Z., Wen, T., Shah, V., Li, K., Moch, J.M., Bates, K.H., Song, S., Shen, L., Zhang, Y., Luo, G., Yu, F., Sun, Y., Wang, L., Qi, M., Tao, J., Gui, K., Xu, H., Zhang, Q., Zhao, T., Wang, Y., Lee, H.C., Choi, H., Liao, H., 2021. Control of particulate nitrate air pollution in China. Nat. Geosci. 14, 389–395.
Zhang, R., Zhang, Y., Lin, H., Feng, X., Fu, T.-M., Wang, Y., 2020. NO_x emission reduction and recovery during COVID-19 in East China. Atmosphere 11, 433.
Zhang, Y., Wu, W., Li, Y., Li, Y., 2023. An investigation of $PM_{2.5}$ concentration changes in Mid-Eastern China before and after COVID-19 outbreak. Environ. Int. 175, 107941.
Zhao, Y., Nielsen, C., Lei, Y., McElroy, M.B., Hao, J., 2011. Quantifying the uncertainties of a bottom-up emission inventory of anthropogenic atmospheric pollutants in China. Atmos. Chem. Phys. 11, 2295–2308.
Zheng, B., Tong, D., Li, M., Liu, F., Hong, C., Geng, G., Li, H., Li, X., Peng, L., Qi, J., Yan, L., Zhang, Y., Zhao, H., Zheng, Y., He, K., Zhang, Q., 2018. Trends in China's anthropogenic emissions since 2010 as the consequence of clean air actions. Atmos. Chem. Phys. 18, 14095–14111.
Zoogman, P., Jacob, D.J., Chance, K., Zhang, L., Le Sager, P., Fiore, A.M., Eldering, A., Liu, X., Natraj, V., Kulawik, S.S., 2011. Ozone air quality measurement requirements for a geostationary satellite mission. Atmos. Environ. 45 (39), 7143–7150.